

Special Section:

Years of the Maritime Continent

Revisiting the Seasonal Cycle of the Timor Throughflow: Impacts of Winds, Waves and Eddies

 Beatriz Peña-Molino¹ , Bernadette M. Sloyan¹ , Maxim Nikurashin² , Océane Richet¹ , and Susan E. Wijffels³ 
¹Centre for Southern Hemisphere Oceans Research (CSHOR), CSIRO Oceans and Atmosphere, Hobart, TAS, Australia, ²Institute of Marine and Antarctic Studies, University of Tasmania, Hobart, TAS, Australia, ³Department of Physical Oceanography, Woods Hole Oceanographic Institution, Woods Hole, MA, USA
Key Points:

- The seasonal cycle of the Timor throughflow is due to a combination of local winds, remotely forced Kelvin waves and non-linear effects
- Inflow from Makassar, divergence in the Banda Sea and locally wind-driven flow increase throughout the Southeast Monsoon (SEM)
- Eddies reduce the volume and heat transport of the Timor throughflow during the peak of the SEM

Supporting Information:

Supporting Information may be found in the online version of this article.

Correspondence to:
 B. Peña-Molino,
bea.pena-molino@csiro.au
Citation:
 Peña-Molino, B., Sloyan, B. M., Nikurashin, M., Richet, O., & Wijffels, S. E. (2022). Revisiting the seasonal cycle of the Timor throughflow: Impacts of winds, waves and eddies. *Journal of Geophysical Research: Oceans*, 127, e2021JC018133. <https://doi.org/10.1029/2021JC018133>

Received 14 OCT 2021

Accepted 28 MAR 2022

Author Contributions:
Conceptualization: Beatriz Peña-Molino, Bernadette M. Sloyan, Susan E. Wijffels

Data curation: Beatriz Peña-Molino, Susan E. Wijffels

Formal analysis: Beatriz Peña-Molino

Funding acquisition: Bernadette M. Sloyan

Investigation: Beatriz Peña-Molino, Bernadette M. Sloyan, Susan E. Wijffels

© 2022. The Authors.

 This is an open access article under the terms of the [Creative Commons Attribution-NonCommercial-NoDerivs License](https://creativecommons.org/licenses/by-nc-nd/4.0/), which permits use and distribution in any medium, provided the original work is properly cited, the use is non-commercial and no modifications or adaptations are made.

Abstract The tropical Pacific and Indian Oceans are connected via a complex system of currents known as the Indonesian Throughflow (ITF). More than 30% of the variability in the ITF is linked to the seasonal cycle, influenced by the Monsoon winds. Despite previous efforts, a detailed knowledge of the ITF response to the components of the seasonal forcing is still lacking. Here, we describe the seasonal cycle of the ITF based on new observations of velocity and properties in Timor Passage, satellite altimetry and a high-resolution regional model. These new observations reveal a complex mean and seasonally varying flow field. The amplitude of the seasonal cycle in volume transport is approximately 6 Sv. The timing of the seasonal cycle, with semi-annual maxima (minima) in May and December (February and September), is controlled by the flow below 600 m associated with semi-annual Kelvin waves. The transport of thermocline waters (<300 m) is less variable than the deep flow but larger in magnitude. This top layer is modulated remotely by cycles of divergence in the Banda Sea, and locally through Ekman transport, coastal upwelling, and non-linearities of the flow. The latter manifests through the formation of eddies that reduce the throughflow during the Southeast Monsoon, when is expected to be maximum. While the reduction in transport associated with the eddies is small, its impact on heat transport is large. These non-linear dynamics develop over small scales (<10 km), and without high enough resolution, both observations and models will fail to capture them adequately.

Plain Language Summary The Indonesian Throughflow (ITF) is a system of currents that connects the tropical Pacific with the Indian Ocean. The strength of these currents varies on scales from days to years. Seasonal changes are large and linked to changes in the Monsoon winds. How exactly the ITF varies with the Monsoon is unclear. Here we investigate the effect of the Monsoon winds on the ITF at Timor Passage (the largest of the outflows) using a combination of observations from moorings, satellites, and high resolution models. We show that winds modulate the ITF remotely through waves generated in the Indian Ocean and changes in sea level of the Banda Sea. Locally winds can accelerate surface currents and drive coastal upwelling, both of which strengthen the ITF. However, the interaction of the strong currents with the complex topography generates eddies, which reduce the volume of water that flows into the Indian Ocean through Timor Passage. As a result the amount of heat delivered to the Indian Ocean when the eddies are present is halved. Low resolution climate models cannot simulate these eddies and may introduce temperature biases in the Indian Ocean that limit our capacity to predict the climate under warmer scenarios.

1. Introduction

The exchange of waters between the tropical Pacific and Indian Oceans occurs through a series of thermocline and intermediate water flows through the complex bathymetry of the Indonesian Seas (Figure 1). Collectively these flows are known as the Indonesian Throughflow (ITF). The ITF transports heat between the two basins, cooling the Pacific Ocean and warming the Indian Ocean. The increase in heat content in the Indian Ocean observed in recent decades has been attributed to an increase in heat transport by the ITF (Lee et al., 2015; Zhang et al., 2018). The volume transport by the ITF is predicted to change under future climate scenarios (e.g., Feng et al., 2018; Hu et al., 2015; Sen Gupta et al., 2016), therefore it is critical to accurately represent the dynamics of the local circulation to properly represent its broad impacts on the climate system.

The mean flow in the ITF is driven by the pressure gradient between the Pacific and Indian Ocean (Wyrтки, 1987), which is maintained by winds in the Indo-Pacific region. Hence variability in these winds may play a role in

Methodology: Beatriz Peña-Molino, Maxim Nikurashin, Susan E. Wijffels
Project Administration: Bernadette M. Sloyan, Susan E. Wijffels
Resources: Bernadette M. Sloyan, Susan E. Wijffels
Software: Beatriz Peña-Molino, Maxim Nikurashin, Océane Richet
Validation: Maxim Nikurashin, Océane Richet
Visualization: Beatriz Peña-Molino, Maxim Nikurashin, Susan E. Wijffels
Writing – original draft: Beatriz Peña-Molino
Writing – review & editing: Bernadette M. Sloyan, Maxim Nikurashin, Océane Richet, Susan E. Wijffels

the ITF strength. One of the largest sources of climate variability over the Maritime continent is the seasonal monsoonal winds. During June–July–August, strong southeasterly winds bring dry air over the Maritime continent. This period is known as the Southeast Monsoon (SEM). During December–January–February, moist winds blow from the northwest comprising the Northwest Monsoon (NWM). As the Intertropical Convergence Zone moves across the equator during the Monsoon Transition months (MTS), westerly wind bursts (often associated with the Madden-Julian Oscillation) over the equatorial Indian Ocean trigger Kelvin waves that propagate into the Indonesian seas. These Kelvin waves provide yet another source of variability for the flow at seasonal and also intraseasonal time scales (Schiller et al., 2010).

In the upper ocean, the effect of the local seasonal winds on the ITF is thought to be regulated through Ekman divergence/convergence cycles over the internal seas (Wyrski, 1987). During the SEM, winds drive divergence and upwelling in the Banda Sea, which enhances the export of water by the ITF. Conversely, during the NWM, downwelling in the Banda Sea results in the storage of upper thermocline water in the internal seas, and reduced ITF transport. Gordon and Susanto (2001) showed that the timing of this upwelling/downwelling cycle is such that upwelling is maximum (2.5 Sv) during May–June, and downwelling peaks (1 Sv) during February. In addition, local winds can also drive changes in the ITF outflows. During the SEM (NWM) winds along the northern side of the Nusa Tenggara island chain produce a southward (northward) Ekman transport that enhances (reduces) the ITF, as shown by Sprintall and Liu (2005).

Quantifying the joint effect of the various elements of the seasonal forcing in the transport of the ITF was not possible until the International Nusantara Stratification and Transport program (INSTANT) in 2004–2006. INSTANT was the first major effort to measure inflow and outflow simultaneously. Of the three major outflows, Lombok, Ombai, and Timor (from west to east), INSTANT data showed that the Timor Passage had the largest and steadiest of the flows, carrying up to half of the ITF (7.5 Sv), but varying by around 5 Sv over the annual cycle (Sprintall et al., 2009). Variability in Ombai Strait, the second largest of the outflows (4.9 Sv) was larger than Timor during INSTANT. However, seasonal changes in the transport in both straits were out of phase (maximum in Ombai during July–August and December–January, and maximum in Timor during April–June), driven by the passing of Kelvin waves. As a result, the total ITF exhibited a smaller seasonal cycle, in contrast with earlier modeling studies that show a large amplitude of the seasonal cycle (>8 Sv, Potemra, 1999) and observations of the seasonal cycle at Makassar strait (>6 Sv, Pujiana et al., 2019).

While observations collected in INSTANT have provided a benchmark for modeling studies and allowed for various proxies of ITF transport to be derived (e.g., Feng et al., 2018; Hu & Sprintall, 2017; Sprintall & Révelard, 2014; Susanto & Song, 2015; Tillinger & Gordon, 2010), the INSTANT record was relatively short and it is unclear if the conditions sampled during INSTANT are relevant for the longer-term mean. Lee et al. (2010) noted both decadal and interannual changes in the ITF in ocean reanalysis products. While INSTANT took place during a relatively neutral state of the El Niño Southern Oscillation and Indian Ocean Dipole cycle, with the first half of the record occurring during weak El Niño conditions, then transitioning to weak La Niña conditions. In addition, the contribution from the circulation on Australia's northwest shelf to the ITF was never measured directly, but was assumed to be small based on the very limited surveys by Cresswell et al. (1993). Long term observations of the shelf circulation are needed to address this question. Observations of the cross-passage structure of the velocity field can also help separate the seasonal variability in transports due to remote (remotely forced coastal Kelvin waves and changes in the storage/discharge in the internal seas) versus local process (e.g., Ekman dynamics).

To gain further insight into the ITF and its seasonal dynamics, and provide an extended record of velocities and property transports across Timor Passage, a 6-mooring array was deployed across the eastern side of Timor between April 2011 and December 2015 funded through the Australian Integrated Marine Observatory System (IMOS) and CSIRO Oceans and Atmosphere. In addition to measurements of the flow, this new record provided high resolution observations of the temperature and salinity across the passage. In this study we combined these new in situ observations with remote sensing data and output from a high-resolution regional model of the ITF to provide revised estimates of the Timor throughflow contribution to the ITF, as well as shed some light on the relationships between inflow, circulation in the internal seas, local dynamics and outflow transports.

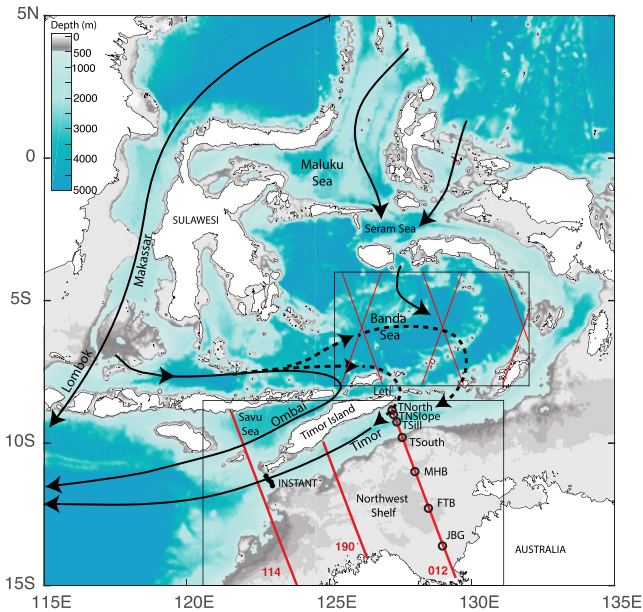


Figure 1. Map of the Indonesian Seas. Black arrows illustrate the mean flow direction, including the separation of the inflow into the eastern (via Seram Sea) and western (via Makassar Strait) pathways, and the outflows into the Indian Ocean, from west to east, through Lombok, Ombai and Timor straits. Dashed lines show the two Timor throughflow sources as proposed in this study: the direct western pathway around the eastern end of Timor and a recirculating route via Banda Sea entering Timor Passage further to the east. Red lines indicate altimeter tracks. These were extracted in the Timor Passage (black box to the south) for geostrophic velocity analysis, and in the Banda Sea to explore the cycles of storage/discharge in the internal sea. Black circles along the eastern most altimeter track in Timor show the location of the Integrated Marine Observatory System moored array. From North to South the mooring sites are as follows: Timor North Slope, Timor North, Timor Sill, Timor South, Margaret Harries Banks, Flat Top Banks and Joseph Bonaparte Gulf. Black dots on the western end of Timor Passage indicate the location of the International Nusantara Stratification and Transport program moorings. Major internal seas are also identified.

2. Data and Methods

2.1. Mooring Observations

The Timor Passage IMOS/CSIRO array was deployed at the eastern end downstream of the Leti Sill (1,250 m) at approximately 127.5°E. The array was oriented in a north-northeast direction more or less normal to local bathymetry between 8.8 and 13.6°S (Figure 1). Three tall moorings occupied the deep part of the passage with the deepest, referred to as the Timor Sill (TSill) mooring, located in the center of the passage in approximately 3,000 m of water, and the other two located at the northern and southern flanks of the passage (Timor North (TNorth) and Timor South (TSouth) respectively in Figure 1). The TSill and TNorth moorings were turned around every 18-month for the duration of the experiment. After the first two deployments, it became apparent that the northernmost mooring was located outside the main jet of the Timor Throughflow, in a “shadow zone”, an area of weak or reversed flow adjacent to the northern boundary. For the remainder of the experiment, the northernmost mooring was moved further south from a depth of 1,100 m into the channel to a depth of 1,600 m (Timor North Slope (TNSlope) in Figure 1). The remaining three shallow moorings were located over the Northwest Australian shelf in water depths ranging from 150 m for the northernmost mooring, to less than 50 m at the southern end of the array. These shallow moorings (Joseph Bonaparte Gulf (JBG), Flat Top Banks (FTB), and Margaret Harries Banks respectively, Figure 1) along with TSouth were maintained by the Australian Institute of Marine Science and turned around on a 6-month schedule.

All six moorings collected measurements of temperature, salinity and horizontal velocity. The exact instrument distribution varied slightly between deployments. Horizontal velocities within the top 700 m in all three tall moorings were obtained by pairing upward and downward looking Acoustic Doppler Current Profilers (ADCP) at approximately 100 m. At this depth the upward looking ADCP signal can travel right through the surface with the mooring standing tall. However, the top two bins were lost due to surface reflection contamination. Below 700 m a series of point measurement acoustic current meters recorded velocities at approximately 200 m intervals all the way down to 1,500 m on the deepest moorings. Due to the depth of the controlling sill upstream, no transport occurs below this level. The shelf moorings consisted of an upward looking ADCP near the bottom.

Temperature measurements were collected by a combination of Temperature-Pressure/Depth (TD, Seabird39), pumped Conductivity-TD (CTD, Seabird37) and compact thermistors (Star Oddi), distributed approximately every 20 m within the top 200 m of the tall moorings, and with progressively lower resolution ranging from 50 to 150 m below 200 m. On the shelf moorings, temperature sensors were distributed throughout the water column from 5 to 20 m apart. Salinities were recorded at lower vertical resolution across the array (3 records available throughout the shelf), and are only used here to produce monthly averaged temperature/salinity (T/S) diagrams for the sill mooring.

Tides in the Indonesian Seas are large, in particular the M2 component. In order to minimize the effect of the tide from the observations, 14 tidal components were fitted to each of the records, and then subsequently removed from the time series. Once de-tided, velocity data were processed in a similar fashion as was previously done during INSTANT data (see Sprintall et al., 2009). That is, first profiles were interpolated into a common 1-hr time base and then linearly interpolated in the vertical to 10 m resolution, and lastly surface gaps due to mooring blow down extrapolated via a linear shear model. This shear extrapolation likely underestimates the contribution from the Ekman flow, as contamination from surface echoes prevents the upward looking ADCPs from fully resolving velocities within Ekman layer. In the remainder of the paper, we will refer to the de-tided interpolated/extrapolated

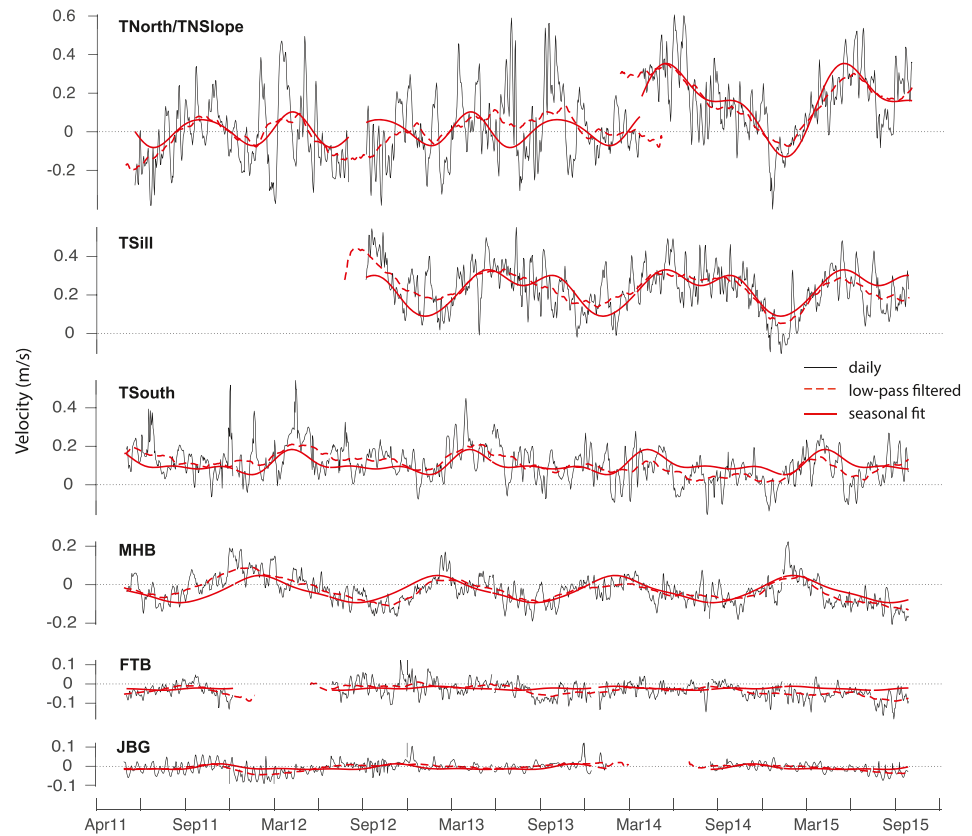


Figure 2. Along-stream velocity at 50 m, from the combined Timor North/Timor North Slope, Timor Sill, Timor South, Margaret Harries Banks, Flat Top Banks and Joseph Bonaparte Gulf from top to bottom. Black lines show raw-data (daily de-tided data), dashed red lines show low-passed filtered data with a 90-day running mean, and in solid red are the results from the 3-harmonic seasonal fit.

data as “raw data”. Finally, we derive the seasonal cycle out of the 5-year time series by fitting three harmonics to the raw data record at each mooring site. At the TNSlope, TSill, TSouth and Margaret Harries Banks mooring sites the harmonic fit is able to accurately separate the repeatable part of the seasonal cycle from shorter- and longer-term variability (Figure 2). The flow at the TNorth, FTB and JBG sites also contains significant energy at annual and semi-annual time scales. However, the signal associated with these time scales at these sites is much less repeatable, and thus the fit probably underestimates the variability at seasonal timescales.

2.2. Satellite Observations

In addition to the mooring data, we also derived surface geostrophic velocities from altimetry. The moored array was collocated with TOPEX/Poseidon and Jason altimeter track number 012. To the west, tracks 190 and 114 also cross the Timor Passage approximately normal to the local bathymetry, with track 114 just slightly downstream, in the ITF sense, from the location of the INTANT moorings (see Figure 1). We use Sea Surface Height (SSH) from X-TRACK distributed by CNES (Birolet et al., 2017), an along track data product specifically processed for coastal applications. This product is individually processed over a series of subdomains. In order to produce continuous transects across Timor Passage, we merged data from the West Australia and South China Sea regions. Both domains overlap in the middle section of Timor Passage. In general, we found data from both domains agreed in the overlapping region, with a few exceptions. At times when they disagreed, we used an average of both domains, which unavoidably introduced noise. To reduce the noise inherent to SSH measurements near coasts and to average through the large internal tidal signals, we applied a 40 km square filter tapered toward the northern and southern ends of the passage. Next, we proceeded with the seasonal fit, also using 3 harmonics. As with the moorings, 3 harmonics was sufficient to accurately represent the annual cycle in SSH. Finally, we computed surface geostrophic velocities of the smoothed seasonal cycle of SSH.

To derive the Ekman transport across Timor Passage we use winds from NASA's Cross-Calibrated Multi-Platform (CCMP) ocean surface wind project (Wentz et al., 2015). We use wind speed Level 3.0 data which has resolution of $\frac{1}{4}$ degree latitude \times $\frac{1}{4}$ degree longitude and is provided 6-hourly. We first projected the data onto the mooring line via linear interpolation, then rotated into the along- and across-transect components, and produce a climatology for the years 2010–2015.

Finally, to extend the mooring temperature data to the surface, we also use sea surface temperature (SST) data from the spatial-scale sea surface temperature atlas of the Australian regional seas (SSTAARS) climatology derived from Advanced Very High-Resolution Radiometer (AVHRR) data (Wijffels et al., 2018). This climatology is generated via harmonic fit to the entire 25-year AVHRR data set. SST is provided in a 1° latitude \times 1° longitude resolution grid, and for the purpose of extending the mooring records to the surface it was simply linearly interpolated to the mooring line.

2.3. Model Output

To explore the dynamics of the Timor throughflow as it navigates the complex bathymetry and turns around the eastern tip of Timor, as well as to guide the interpolation of the mooring data, we use horizontal velocity fields from a 10 km and a 1 km resolution regional model of the ITF. The model simulations are based on the MITgcm (Marshall et al., 1997) over a domain with approximate boundaries at latitudes 10°N and 15°S and longitudes 107°E and 139°E . Both simulations have 100 vertical levels with varying resolution from 2 m near the surface to 200 m at depth. The model is run in hydrostatic configuration with KPP mixing and it is forced by monthly averaged fields derived from a repeat year forcing (May 1984–April 1985) run by the Consortium for Ocean-Sea Ice Modeling in Australia (COSIMA, <http://cosima.org.au>). COSIMA fields are applied both at the open boundaries and at the surface by restoring to temperature and salinity over a 3-day time scale. The 10 km resolution model is run for 12 years. Resolution is then scaled up by initializing progressively higher resolution models, from 10 to 4 to 1 km, with output from the lower resolution model interpolated into the higher resolution grid and run to equilibrium. At 1 km resolution the model was run for 2 years and reached equilibrium after 6 months. For both resolutions model fields are saved every 10 days, and only the last year is used for the analysis presented here.

The regional model has some inherited biases from the forcing fields (see Kiss et al., 2020 for further details), these affect primarily the temperature and salinity distribution. Here, we are interested in the structure of the velocity field. The model's velocity field compares well with observations (Figures S1 and S2 in Supporting Information S1), and the time mean transports at the inflow and outflow passages are within the range of observed values. However, the partition of the transport between the two resolutions is different. In the 1 km model more of the transport enters the Indian Ocean through the smaller passages (Lombok and Ombai), which are better resolved at the higher resolution, and less through Timor.

2.4. Gridding of Mooring Data

One of the largest sources of uncertainty in the transports estimated from INSTANT was the interpolation/extrapolation of the mooring data across the passage (Sprintall et al., 2009). Our approach here to determine an appropriate gridding scheme was based on the observed cross-passage structure from altimetry-based surface geostrophic velocities and SST, but also guided by analysis of the flow structure of the 1 km high resolution regional model of the Indonesian Seas.

The mapping proceeded as follows. We first created a 2-dimensional distance-depth regular grid using bathymetry from ETOPO1 (Amante & Eakins, 2008) along the mooring line. Across the Timor Passage where the topographic slope is steep and the flow is expected to change over short length scales, the grid had 1 km resolution. In the shelf, where moorings were further apart, and topography variations are gentler, the grid transitions to 5 km resolution. The flow was assumed to be 0 at the grid cell closest to the wall, that is 1 km away from the actual boundary. There are no actual observations of the flow near the boundaries to guide our selection of boundary conditions. Our choice instead is consistent with the no-slip condition in the regional model and also consistent with the treatment of the data from the INSTANT moorings. To interpolate between the boundary and the mooring sites, we tested three methods: linear interpolation, natural-neighbor interpolation, and optimal interpolation with various choices of decorrelation scales. For each case we subsampled the 1 km resolution regional model in a similar fashion to the moorings, and re-gridded the data with each of the methods. Comparing the exact

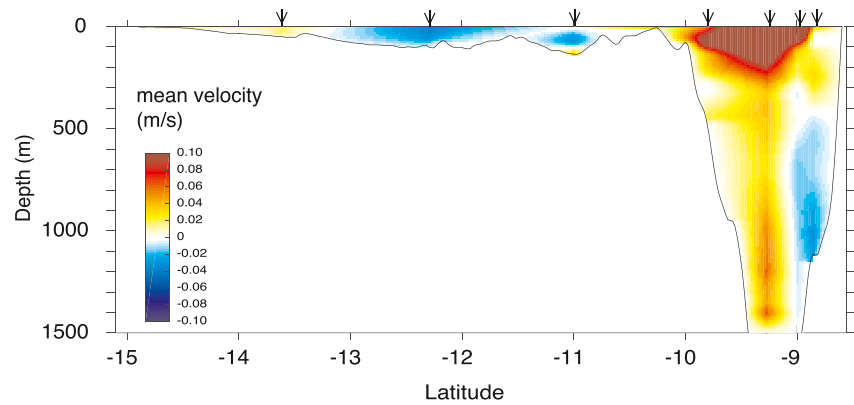


Figure 3. Gridded time mean velocity (cm/s) section. Positive values indicate flow to the southwest (toward the Indian Ocean), negative to the northeast. Arrows along the top axis indicate the position of the moorings.

transport from the model with the re-gridded version we found that natural-neighbor interpolation produced the most realistic transports, with maximum errors of up to 1 Sv in the transports for the 10 days snap shots and errors in the time mean transports of less than 5%. The model, however, lacks interannual variability and in addition to the interpolation error, we also expect a sampling error due the relocation of the northern mooring after the second deployment.

The time-averaged along-stream velocity (Figure 3), derived from the above mapping, provides context for the velocity anomalies that will be discussed below. The time mean Timor throughflow is to the southwest (positive) through most of the deep portion of the passage (red in Figure 3), with the exception of the flow along the northern flank below 500 m depth. The core of the mean throughflow is confined to the main thermocline within the top 300 m, but significant flow occurs at depth, with a secondary core between 1,000 and 1,500 m. On the Australian shelf, the mean circulation is primarily to the northeast opposing the ITF.

The temperature data was processed in a similar way to the velocity and gridded using boundary conditions consistent with the no-slip condition applied to the velocity field—that is, we imposed a zero cross-strait temperature gradient at the boundary. Finally, temperature values were interpolated between the surface and the upper most record at each mooring site by using the SSTAARS climatology.

3. Results

3.1. Seasonally Varying Surface Geostrophic Flow From Altimetric Measurements

Due to contamination by surface reflections in the ADCP data, our moorings cannot measure the very near surface flow. Thus, we characterize the near surface flow across and along the Timor Passage over the seasonal cycle through a climatology of the surface geostrophic anomalies derived from the along-track altimeter data (Figure 4). We expect the geostrophic circulation to be representative of the upper ocean (top 100 m) below the Ekman layer. Within the Ekman layer the actual circulation is a combination of the Ekman flow, only partly resolved by the array, and the geostrophic flow described here. We define geostrophic anomalies with respect to the 25+ year altimeter record. Here and throughout the paper unless otherwise specified, positive values represent velocities directed to the southwest (favoring the ITF), negative anomalies to the northeast (reducing the ITF).

The annual cycle of the surface geostrophic flow is dominated by a strong but short reduction of the ITF centered over the deep axis of the Timor Passage during the peak of the NWM (December-March) and a longer period of positive anomalies with smaller magnitude that reinforce the ITF during the remaining of the year. The transition toward a stronger ITF begins close to the northern boundary at the eastern most track in April, and progressively moves westward and extends across the deep passage. By June the positive anomalies are located over the deepest part of the passage on all three tracks. In July the flow in the eastern most track develops the so called “shadow zone”, an area of weak or reversed flow adjacent to the northern boundary. This shadow zone likely develops due to the inertia of the strengthening Timor throughflow jet as it rounds the eastern end of Timor island near 128°E. As the jet strengthens and its inertia increases, the jet axis progressively moves southward. Note this effect is

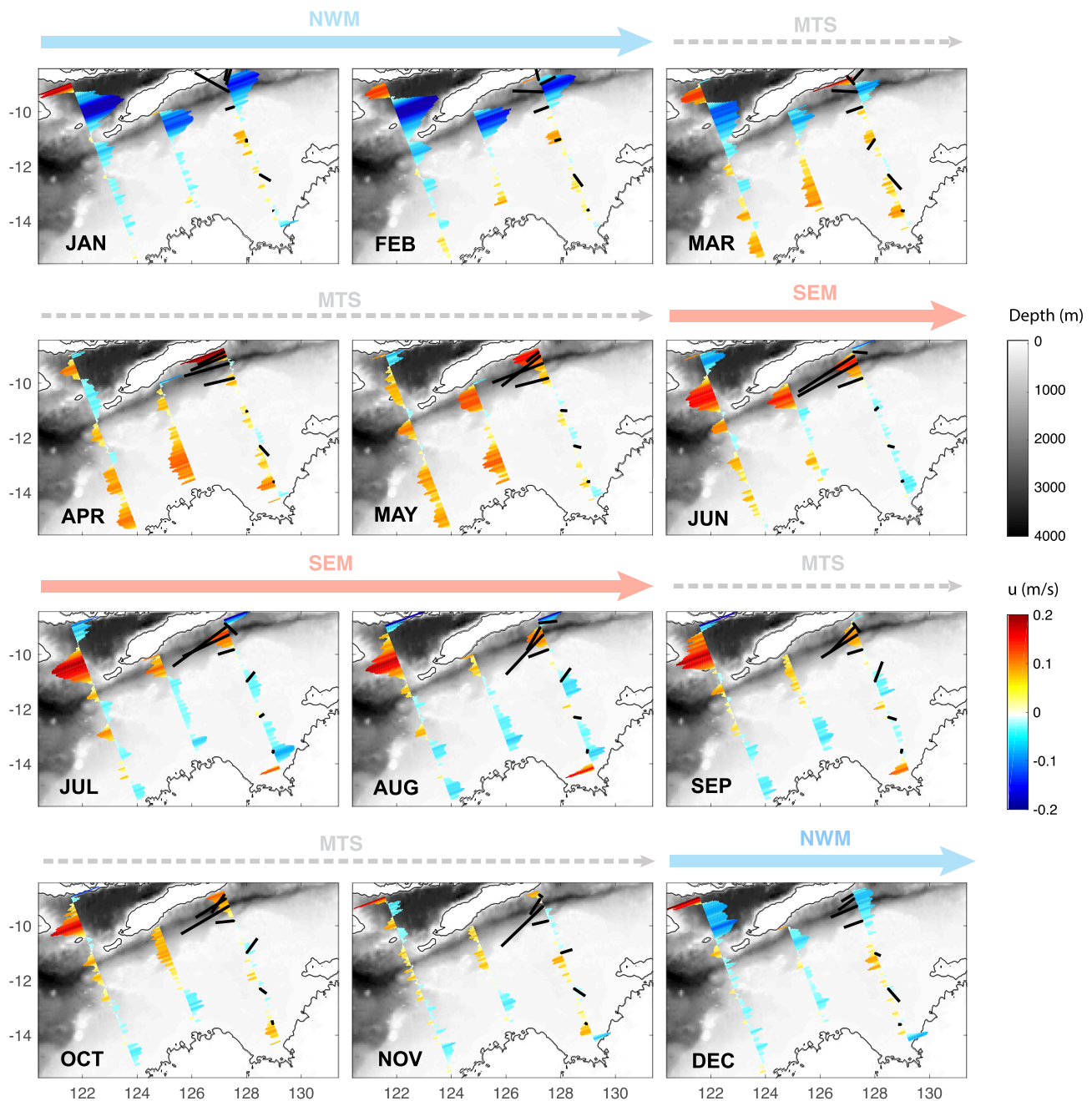


Figure 4. Monthly means of surface geostrophic velocity anomalies (m/s) derived from along track altimeter data superimposed on bathymetry (in gray) in Timor Passage and Savu Sea. Velocities are normal to the track and anomalies defined positive (warm colors) when they are to the Southwest (strengthened Indonesian Throughflow (ITF)), and negative (cold colors) to the northeast (weaken ITF). Both color and vector length indicate the magnitude of the flows. Monthly means are defined over the full altimeter record mean (see text for details on the processing). Also shown in black are monthly averaged full velocity vectors (mean plus anomalies) at 50 m in each mooring site. These are obtained by averaging the raw data over the entire mooring record. For context the various phases of the monsoon cycle (Northwest Monsoon, Monsoon Transition months (MTS), and Southeast Monsoon) are also shown at the top of each panel.

not evident in the opposite season (December – March) when the seasonal flow weakens the Timor jet. We will discuss this aspect of the circulation in more detail in Section 3.4.

The maximum in the positive geostrophic anomalies on the eastern most track, where the moorings are located, is always found near the Tsill site. However, during April and May, the flow anomalies are split into two different cores: a primary one slightly displaced to the north of the deep sill, and a secondary one along the southern flank

in the deep passage, centered around the TSouth mooring site. Temperature and salinity data collected at this location show waters with very different properties to those found in the mooring sites to the north (not shown). This suggests that the waters within this secondary velocity core could have a different source region, such as the eastern Banda Sea via a direct flow from the east, rather than a source north of Timor Island.

Also evident in the surface geostrophic velocity anomalies is the tendency for the flow on the Australian Northwest Shelf during the SEM to be out of phase with the flow in the deep portion of the passage, suggesting some recirculation may exist between the shelf and southern flank of the ITF. During July and August, in the peak of the SEM, velocity anomalies are predominantly negative, indicating reduced or reversed flow during this period. In the shelf stronger flow in the ITF sense occurs between March and May consistent with the timing of the sea level pulse that results from the monsoon driven buildup of sea level in the Gulf of Carpentaria and moves westward through the region as described by Ridgway and Godfrey (2015). We will show later that the annual cycle in transport across the shelf derived from direct observations of the flow follows a similar pattern, contrary to previous work that describes the circulation as primarily Ekman driven, with the flow directed to the west most of the year, and weak westward to eastward flow occurring during the NWM (Cresswell et al., 1993; Schiller et al., 2010).

The geostrophic flow to the north of Timor Island, in the Savu Sea, connects the outflow from Ombai Strait to the Indian Ocean. Its seasonal cycle is more or less consistent with that observed in the Timor Passage. The magnitude and phasing of the strong reduction of the southwestward flow (negative anomalies) during the NWM is similar across both passages, though the peak in the SSE velocity is slightly out of phase between both straits. While Timor's surface velocity peaks in May-June, that through Ombai is largest during July-August-September. The lag between the velocities in the two straits, could indicate that reduced flow in the Timor Passage contributes to the enhancement of that in Ombai, a concept that is often referred to as "gating" (e.g., Sprintall & Révelard, 2014; Sprintall et al., 2019). We will show later that the near surface transport in the Timor Passage decreases after June due to non-linearities of the flow. This blocked transport could explain the later seasonal peak in Ombai Strait.

It is also interesting to note that at the western most altimeter track in the Timor Passage, near the original location of the INSTANT array, the variations in the seasonal flow are relatively weak compared to those found upstream. This is consistent with the smaller amplitude of the seasonal cycle described from the INSTANT observations (approximately 3 Sv, Sprintall et al., 2009) compared to that reported here.

3.2. Gridded Velocity Climatology and Transport

The seasonal changes in along-strait velocity anomalies derived from the moored array are complex and vary dramatically throughout the year (Figure 5). In the vertical we find a three-layer pattern. The near surface flow anomalies peak during the May-June period, and reach minimum values in January-February, consistent with the sea level anomaly analysis. Anomalies in the lower thermocline (200–400 m depths) are often opposite to those near the surface, though there is significant change in the structure across the passage. At depths greater than 400 m, in subthermocline waters, velocity anomalies show a semi-annual signal, with maxima in the May-June and November-December periods, and minima during January-February and July-August. A similar semi-annual signal was found at the western end of Timor Passage during the INSTANT program (Sprintall et al., 2009).

Integrating the alongshore total velocity (mean plus anomalies) between Timor Island and Australia, we derived the seasonal cycle of the volume transport (Figure 6a). Transport is a maximum (8 Sv) during May, in the early part of the SEM. The minimum occurs in September, with a transport of 2 Sv. Building on Gordon et al. (2019) classification of waters in Makassar Strait we separate the transport into 3 vertical layers. The top layer, between the surface and 300 m, containing the core of the North Pacific Intermediate water (NPIW). The second layer includes waters also from Makassar Strait but below the core of the NPIW, here defined between 300 and 600 m to avoid the signature of the Kelvin waves as will be described next. And last the deep layer below 600 m primarily containing South Pacific waters.

Comparing the total transport with the layer estimates we find that the seasonal change in total transport is modulated by the transport of the deep flow (below 600 m), which is characterized by a strong semi-annual signal. The deep flow is suppressed in February-March and reverses (–1 Sv) during August-October, and peaks both during May-June and December-January (roughly at the beginning of SEM and middle of the NWM). This semi-annual

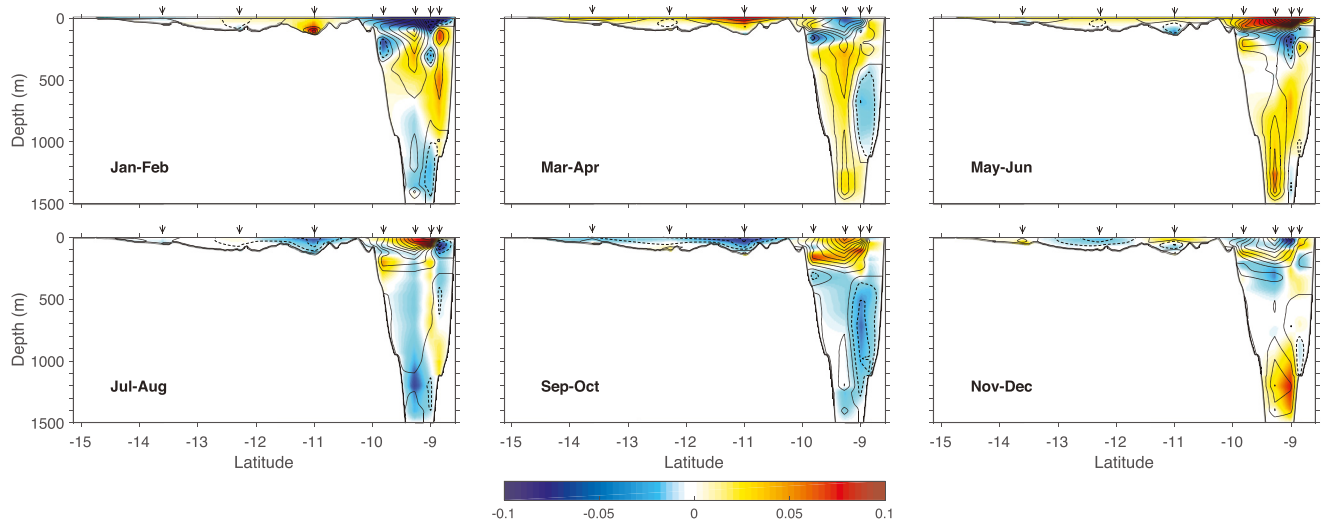


Figure 5. Climatology of the along-stream velocity (m/s). Anomalies are shown in color, and the corresponding absolute velocities by the contours (contour interval is 0.03 m/s). The latter help illustrate when negative anomalies are sufficiently large to reverse the mean flow. Red/warm colors and solid black contours indicate southwestward flow. Black dashed contours and blue/cold indicate velocities to the northeast. Arrows along the top axis show the location of the moorings.

deep flow reversals are the signature of downwelling Kelvin waves as indicated by their typical upward phase propagation (downward energy propagation; Figure 6b). Wind reversals in the equatorial Indian Ocean during the MTS excite Kelvin waves that travel as coastally trapped waves once they reach the coast of Sumatra (Clarke & Liu, 1993; Sprintall et al., 2000). Their energy reaches Lombok in as early as 20 days, and while some of this energy leaks into the internal seas through the strait, the rest continues along the continental slope of the Nusa Tenggara island chain (Drushka et al., 2010; Potemra et al., 2002). As the waves continue to propagate both vertically and horizontally they produce further flow reversals at different depths in different straits. At Timor Passage the Kelvin wave energy is first observed arriving in May at depths of 1,800 m and progressively extending to 600 and (Sprintall et al., 2009). At depths shallower than 1,500 m, the deepest record in our moored array, the May Kelvin wave is not observed until June (Figure 6b), as a result of the phase propagation (e.g., Drushka et al., 2010).

The transport between 300 and 600 m at Timor, containing both lower thermocline and intermediate water, is small, despite the large lateral gradients in velocity across the layer (Figure 5). Transport in the intermediate layer is dominated by the first harmonic, with maximum occurring during the NWM and minimum toward the end of the SEM. This layer is too deep to be influenced by local near surface processes and is too shallow for the deep Kelvin wave energy that reaches the Timor Passage (depths greater than 600 m; Sprintall et al., 2009). As a result, the seasonal cycle in this intermediate layer maybe more directly linked to changes in the circulation of North Pacific water from Makassar strait. We will show later that within this intermediate layer in Timor Passage there are quite distinct seasonal changes in T/S, with a cycle of formation (erosion) of the salinity minimum in July/August (January/February). These seasonal changes in T/S suggest that during the SEM (NWM) Makassar waters may follow a more (less) direct route to Timor and be subject to less (more) recirculation in the Banda Sea.

Within the upper layer (<300 m) the integrated transport of the Timor throughflow is mostly steadier than the deeper flow below. However, the magnitude of the fluctuations in the velocity in this depth range is the largest across the array (Figure 5). The sign of the monthly velocity anomalies within this upper layer varies in depth, with the velocity anomaly below 150 m often being opposite to the anomaly above. On interannual time scales the same was observed in the INSTANT data (e.g., Sprintall & Révelard, 2014; Sprintall et al., 2009). On seasonal time scales, the outflow in the upper 150 m is thought to be regulated by cycles of divergence in the Banda Sea (Wyrtki, 1987). Thus, next we separate the contribution to the upper layer transport above 150 m and below 150 m as well as the contribution from the shelf located approximately at 10°S at the longitude of the moored array. The latter is likely modulated by local processes as opposed to Banda Sea dynamics.

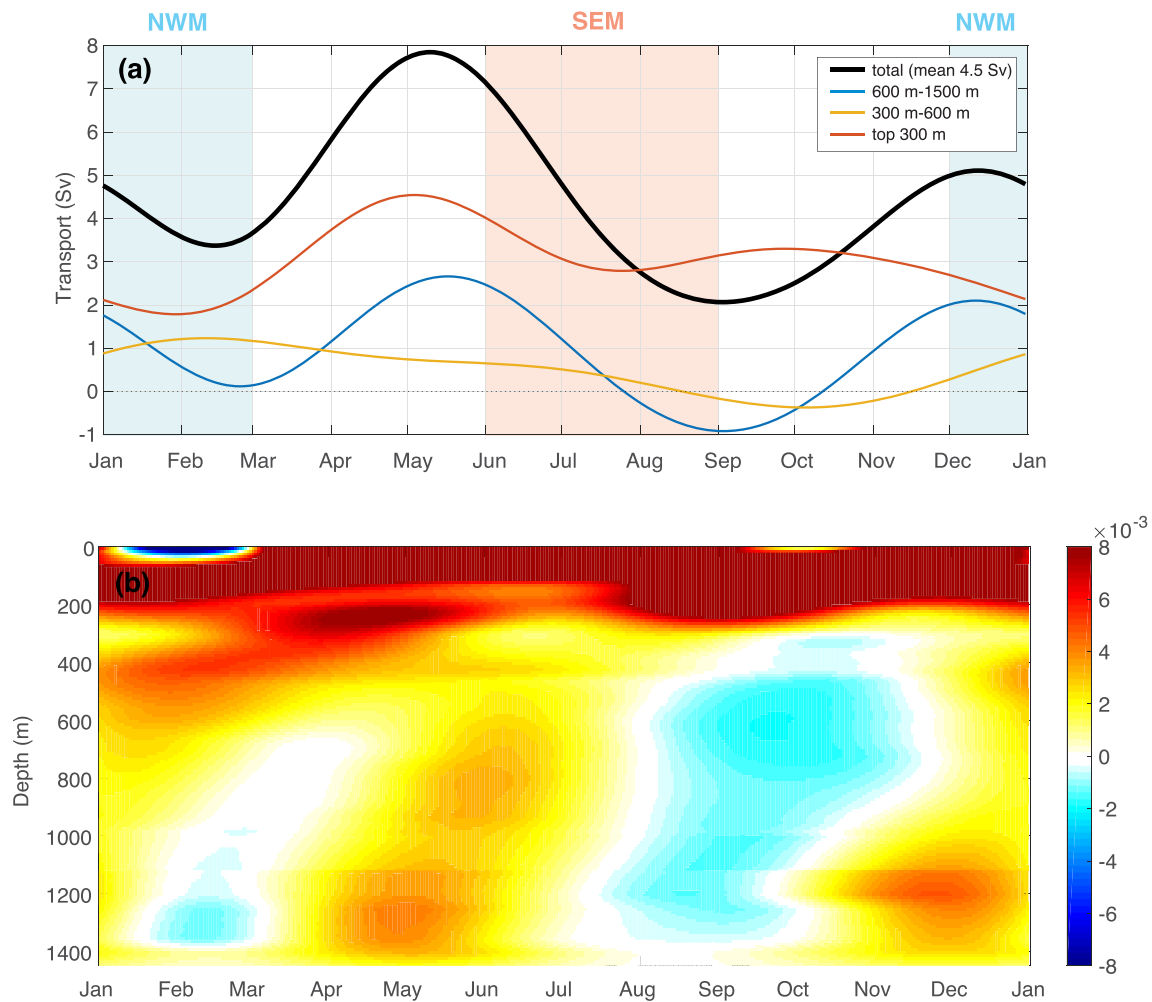


Figure 6. Seasonal cycle of the transport across Timor Passage as observed by the moored array. (a) Transport (Sv) integrated across layers. The black line shows the top-to-1500 m transport, while colors show integrals across the surface, mid and deep layers. Orange and blue shading illustrate the periods of the different monsoon seasons. (b) Transport per unit depth (Sv m^{-2}) showing upward phase propagation of Kelvin waves in the deeper part of the water column.

The amplitude of the seasonal cycle of the shelf transport (south of 10°S) is in general small (Figure 7). Transports are to the southwest favoring the ITF during March-April-May carrying 0.4 Sv at most, and to the northeast in the remainder of the year, with a peak value of 0.8 Sv in October, opposing the ITF. As a result of this asymmetry, the record averaged transport over the shelf is small and directed to the northeast (0.27 Sv). The seasonal evolution of the transport observed here is consistent with early observations by Cresswell et al. (1993), however the timing of the flow reversal is not. Here the flow reverses as early as mid-June, while in Cresswell the reversal is not observed until September. These differences could in part be due to the Ekman flow, which is not fully resolved by the moorings. We will address this in the next section.

Within the deep passage the transport between 150 and 300 m is small (under 1 Sv) and relatively steady. Most of the upper ocean transport occurs through the top 150 m of the water column. There are two maxima in the seasonal cycle of transport between 0 and 150 m, one during May-June and a later one in October-November, both of them in excess of 3 Sv. The minimum occurs in February. As we saw in the velocity sections, changes in transport in the two layers opposed each other: when the transport in the top layer increases, the transport below decreases and vice versa (Figure 7). However, the total transport of thermocline waters is dominated by the much larger top layer transport. We will focus next on the various mechanisms contributing to the upper ocean Timor throughflow, including the Ekman flow which is not fully resolved by the moored array.

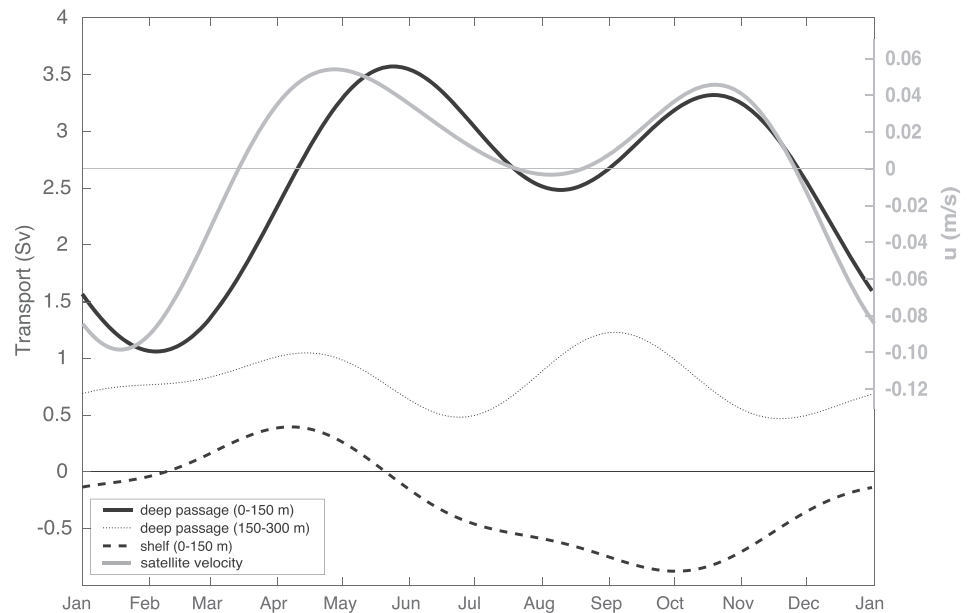


Figure 7. Upper layer transport (<150 m) through the moored array. The deep passage (north of 10°S) transport is shown in solid black, and the shelf portion of the array (south of 10°S) in dashed black. For completeness the transport between 150 and 300 m in the deep passage is also shown (black dotted). Surface geostrophic velocity anomalies averaged north of 10°S for altimeter track 012 are shown in the right axis in gray.

3.3. Local Winds

To estimate the Ekman transport normal to the mooring line we focus first on the component of the winds parallel to the mooring line along the north-northwest/south-southwest (NNW/SSE) direction. A wind directed toward the north will produce westward transport in the Ekman layer, favoring the ITF, while winds directed to the south will produce eastward Ekman transport acting to reduce the ITF. The seasonal cycle of NNW/SSE wind over the entire Timor Sea is strongly asymmetric. Between April and August winds are to the NNW over the entire Timor Sea (Figure 8), weakly to the SSE in January and February, and weak and divergent in March and September–December. As a result, Ekman transport integrated along the mooring line is positive (westward) between April and September, with a maximum value of 0.6 Sv in June–July, and very weak and negative (eastward) during the remainder of the year. There is no semi-annual signal in the Ekman transport, and the timing of the maximum, when compared to the seasonal cycle of the 0–150 m transport inferred from the moorings, confirms the moored array did resolve the Ekman flow. Compared to previous estimates of the contribution of the Ekman transport to the ITF, 5 Sv into the Indian Ocean collectively by all outflows along the Nusa Tenggara island chain (Sprintall & Liu, 2005), suggest that the Ekman flow is relatively weak in the Timor Passage. Nevertheless, our estimates are comparable to early estimates across the Arafura Sea by Godfrey and Mansbridge (2000).

Despite the small size of the direct Ekman effect, the impact of local winds on the Timor throughflow can also occur through coastal upwelling. As Figure 8 illustrates the winds are not directed onshore. The along shore component of the winds during the SEM is much larger than that in the normal direction, and can drive onshore-offshore Ekman transport. When the Ekman transport is directed offshore, coastal upwelling can occur along the Nusa Tenggara island chain and extend to Timor. Raw velocities from TNorth/TNslope and TSill at 50 m show a hint of this offshore Ekman flow (Figure 4). Under favorable coastal upwelling winds, isopycnals tilt upwards toward the coast, SSH is depressed and an alongshore flow develops. In the case of Timor, the SEM winds will drive a jet that further increases the ITF. Typically, the along shore component of the winds during the SEM months is upwelling favorable on the southern side of the Nusa Tenggara and Timor Island (upwelling favorable on the northside of Timor Island during the NWM). And so, a figure illustrating which period of the year the alongshore component of the wind will favor upwelling (not shown) and hence stronger ITF will look much the same as Figure 8, albeit with stronger magnitude.

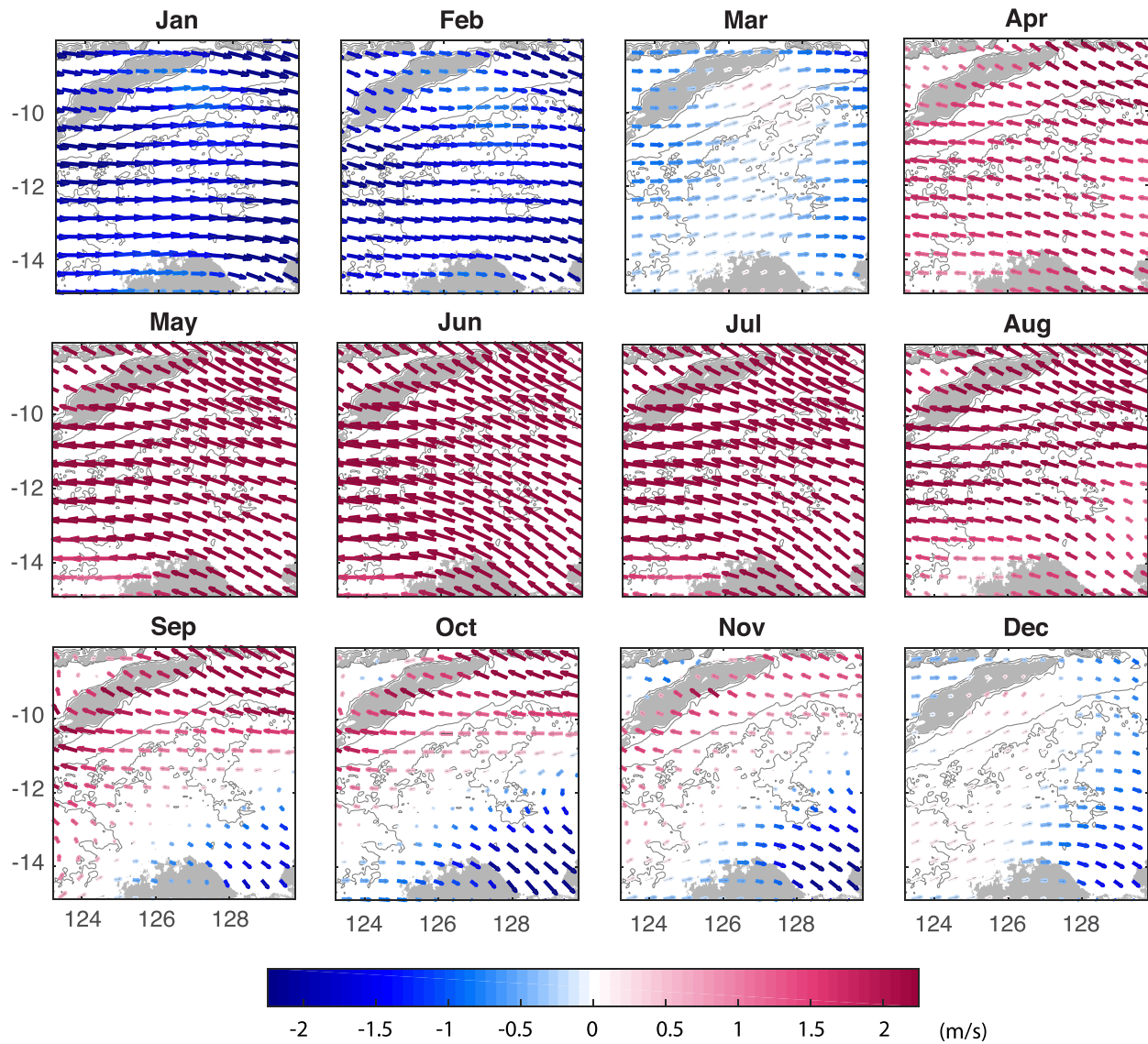


Figure 8. Top: monthly mean wind vectors in Timor Sea. Vectors are color-coded according to the magnitude of component parallel line to the mooring line north-northwest/south-southwest (NNW/SSE) and expressed in m/s. This component can drive Ekman flow normal to the mooring line. Positive (warm tones) indicate winds directed to the NNW when the resulting Ekman transport favors the Indonesian Throughflow, and negative (cold shades) when otherwise. Bottom: Ekman transport integrated from land-to-land across the mooring line. Positive indicates transport to the SSE, and negative to the NNW. The thin black line shows daily values obtained from winds averaged between 2011 and 2015, the gray curve after applying a monthly low-pass filter.

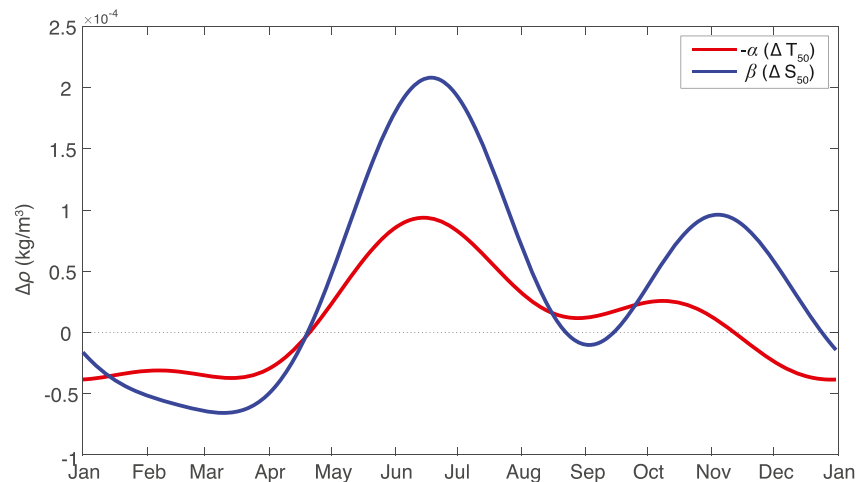


Figure 9. Temperature (red) and salinity (blue) difference at 50 m depth between the Timor Sill and the Timor North moorings. The northern mooring is consistently colder and saltier than the sill site during the peak upwelling season. The timing of this signal is consistent with changes in the wind. During Northwest Monsoon, the opposite is true. Temperature and salinity have been scaled by the thermal expansion, α , and the haline contraction, β , coefficients respectively. Values expressed as a density difference in kg/m^3 .

While the heat transported by ITF is thought to suppress the cooling effect of coastal upwelling along the Java-Sumatra coast (Murtugudde et al., 1998; Qu et al., 1994), the presence of upwelled waters between April and November is easily identified both in SST (Wijffels et al., 2018) and chlorophyll (Susanto et al., 2006). West of Timor along the southern side of the Nusa Tenggara island chain, coastal upwelling is known to modulate the ITF on interannual time scales via changes in the tropical Indian Ocean (Feng & Meyers, 2003). In the Timor Passage, however, surface evidence of coastal upwelling is much less clear, possibly due to the strong control on SST by air sea fluxes. Dry continental winds that blow over the ocean produce large latent heat fluxes during the SEM months and drive cooling over the Timor Sea. Between September and March latent heat loss is small, but shortwave radiation is large, leading to a strong heat flux into the ocean, and warming over the entire sea (e.g., Godfrey & Mansbridge, 2000). As a result, there is little cross-passage structure in SST in the Timor Passage (Wijffels et al., 2018). However, below the surface, the isopycnals tilt upwards toward the coast between April and November, as illustrated by the temperature and salinity gradients between the TSill and TNorth moorings at 50 m depth (Figure 9). Temperature and salinity gradients are maximum between June and July, when velocities at 50 m at the TNSlope mooring are also maximum (Figure 4) and the winds are the strongest, suggesting that local winds can further enhance the upper throughflow in Timor Passage.

3.4. Remote Winds and Non-linearities

The bulk of the inflow of thermocline waters enters the Indonesian Seas through Makassar Strait. The seasonal evolution of the inflow in the top 300 m in Makassar is regulated by the Indo-Pacific pressure difference, and is maximum during July-August and a minimum in December-January (e.g., Gordon et al., 2019; Pujiana et al., 2019). The lag between the maximum inflow and outflow through the exit passages implies, as first described by Wyrki (1987) and later confirmed by others (Gordon & Susanto, 2001), that the internal seas must store and discharge water over certain periods. Near surface transport into the Indian Ocean was found to correlate with Banda Sea surface divergence inferred from altimeter with a 3-month lag. In their analysis Gordon and Susanto find maximum divergence (convergence) occurred during April/May (October/November).

Focusing on the top 150 m of the Timor throughflow (north of 10°S , Figure 7), excluding the shelf portion of the array, we find a much more complex structure of the flow than that expected from the convergence/divergence cycle described above. A maximum transport of 3.5 Sv occurs in May-June, only 1 month after the period of maximum divergence estimated by Gordon and Susanto (2001). This maximum in export is followed by a rapid decrease in transport that leads to the secondary record minimum in mid-August. In September there is a moderate recovery in transport, reaching a secondary maximum in late October/early November. The overall minimum,

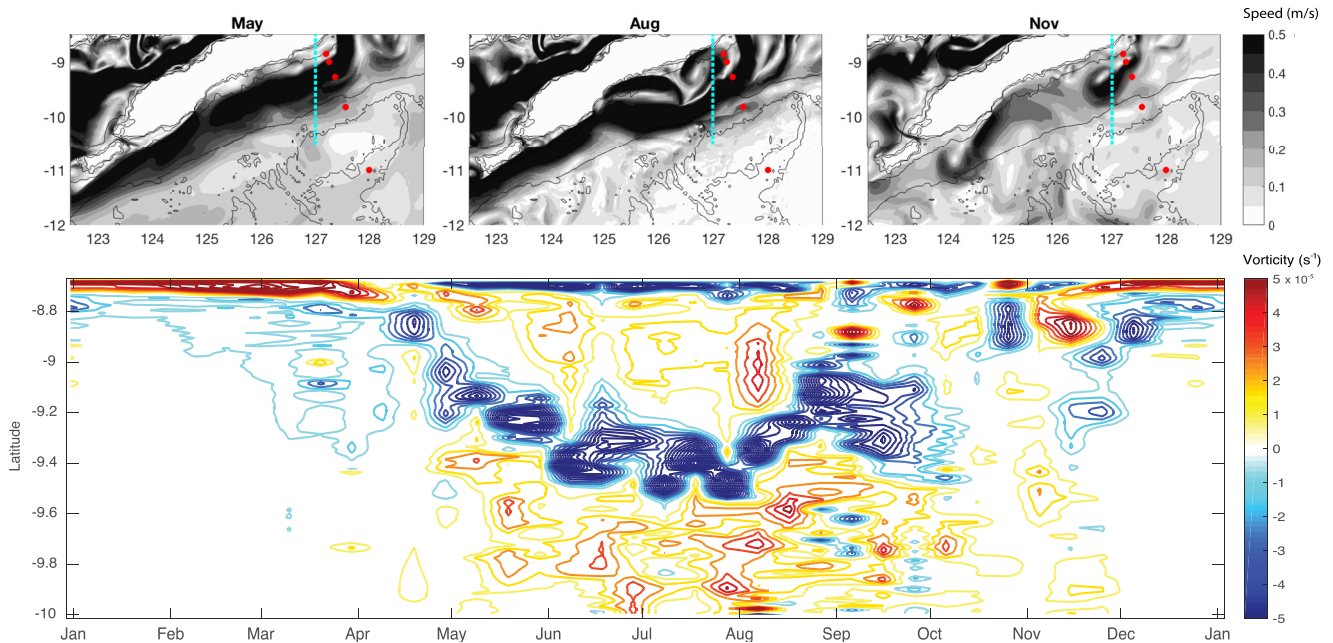


Figure 10. (Top) Surface speed snapshots illustrating the cycle of eddy formation in the 1 km resolution model. (Bottom) Relative vorticity (in s^{-1}) at $127^{\circ}E$ within the deep passage (north of $10^{\circ}S$), along the dotted cyan line in the upper panels. Red dots in the upper panels show the location of the moorings.

of just 0.5 Sv occurs in February in good agreement with Gordon and Susanto's estimate of the lagged relationship between convergence and reduced export. The timing of the various transport maxima and minima inferred from our mooring data is in good agreement with the surface geostrophic flow derived from the altimeter over the same part of the transect (north of $10^{\circ}S$), with some small differences in the magnitude and timing of the peaks, likely due to effect of interannual variability and the much longer length of the altimeter record.

To shed light into the dynamics responsible for this pattern in the upper circulation of the Timor throughflow, we turn next to the numerical model. Snapshots of the surface speed for the modeled Timor Passage during June–November show that as the strength of the ITF increases the flow turning around the eastern tip of Timor becomes more non-linear (Figures 10 and 11). Relative vorticity of the surface flow in the vicinity of the moored array show that non-linearities reach a maximum between June and August. After this time the flow begins to shed eddies that are trapped between the northern edge of the ITF flow and the southern coast of Timor Island. While both resolutions are able to capture the increase in relative vorticity during the SEM, eddies only develop in the 1 km resolution model. The effect of the eddies is two-pronged. In one hand, due to the curvature term the flow develops a strong ageostrophic component that acts to reduce the overall flow. This ageostrophic flow opposing the ITF is a maximum in August, when the eddies are fully developed (Figure 12). In the mooring observations, the eddies are evident as strong intraseasonal flow reversals at the norther sites (Figure 2).

The second, but most important effect we propose, is that throughout the period when the eddies are actively forming, they reduce the net transport by continuously recirculating part of the inflow toward the east along the passage's northern flank. This can be seen by comparing the evolution of the deep passage transport in the top 150 m in both resolutions (Figure 13). Between January and May, transport in both models increases at the same rate. However, in June, when the 1 km model begins to produce eddies the transport stabilizes and oscillates around its peak value throughout the rest of the SEM and into the MTS. In contrast, in the 10 km model, in the absence of eddies, the transport continues to increase reaching its maximum value in July, when the winds are the strongest. The transport captured in the eddies is released as they propagate westward along the passage, explaining the small changes in transport throughout the SEM. However, the narrow continental shelf to the north of the deep passage where the eddies develop is virtually non-existent past $125^{\circ}E$, at which point the eddies can no longer propagate and must instead dissipate locally, likely via friction along the steep vertical walls. By the end of October eddies have for the most part dissipated, but the winds over the Banda Sea still favor discharge (Figure 13, and see also Figure 2a in Gordon & Susanto, 2001) and could explain the secondary maximum in the

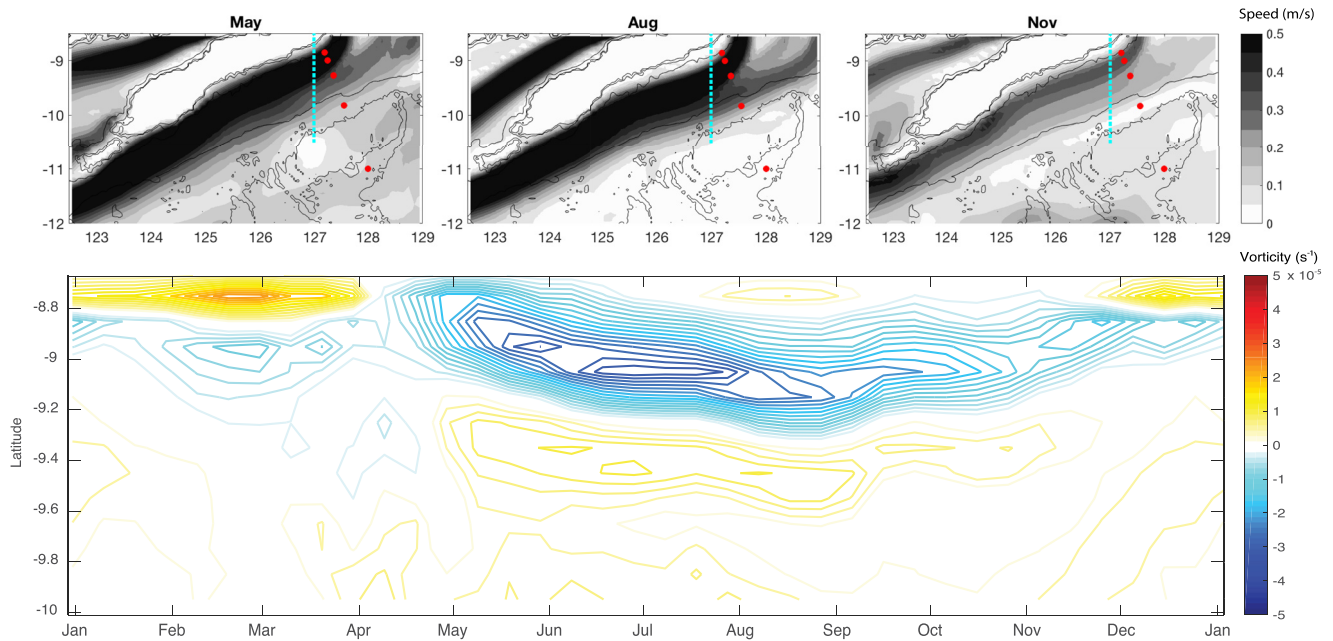


Figure 11. Same as in Figure 10 but from the 10 km resolution model.

observations. This secondary transport maximum is not well reproduced by the model, possibly due to the lack of interannual variability in the repeat year forcing and the proximity of the Timor Passage to the model open boundaries.

4. Discussion

4.1. Connectivity With Banda Sea

To provide context for our observations we now revisit the cycle of convergence-divergence as proposed by Gordon and Susanto (2001). In their study Gordon and Susanto (2001) estimated that over 80% of the variability in SSH can be attributed to mass divergence in the Banda Sea. Like them, we use SSH, in our case along-track data from the X-TRACK product, to characterize the divergence cycle, and compare it to the wind forcing over the Banda Sea and observations of the Timor throughflow.

We first estimate the time rate of change of SSH averaged within the Banda Sea (see definition of Banda Sea in Figure 1), noting that here, as opposed to Gordon and Susanto (2001) we are not converting SSH to layer volume, though the two are linearly related. The time rate of change of SSH is negative (indicating upper layer divergence) from May to September, and it is at its maximum during June-July-August (Figure 14). Wind stress curl estimated from CCMP winds and averaged over the same area is negative favoring upwelling between April and November, and positive (downwelling) during the rest of the year. Maximum upwelling occurs during May-June, leading the peak in SSH changes by approximately 1 month.

Transport in the top 150 m of the moored array increases from late February onwards (Figure 7). This increase in transport cannot be supplied by Banda Sea waters, since between February and May the Banda Sea is still “storing” water, as shown by the positive time rate of change of SSH and negative wind stress curl. On the other hand, the inflow of thermocline waters (<300 m) in the ITF occurs primarily through the western route (e.g., Gordon & Fine, 1996) via Makassar Strait. Transport in Makassar increases between January and August (Figure 4a in Gordon et al., 2019). In January the time rate of change in SSH in the Banda Sea is highest, and though it remains positive until April its magnitude decreases, indicating the Banda Sea is progressively storing less water throughout this period. If the inflow of waters from Makassar continues to increase while the rate of storage in the Banda Sea decreases, a fraction of the inflowing waters must be exported directly into the Indian Ocean without recirculating in the Banda Sea.

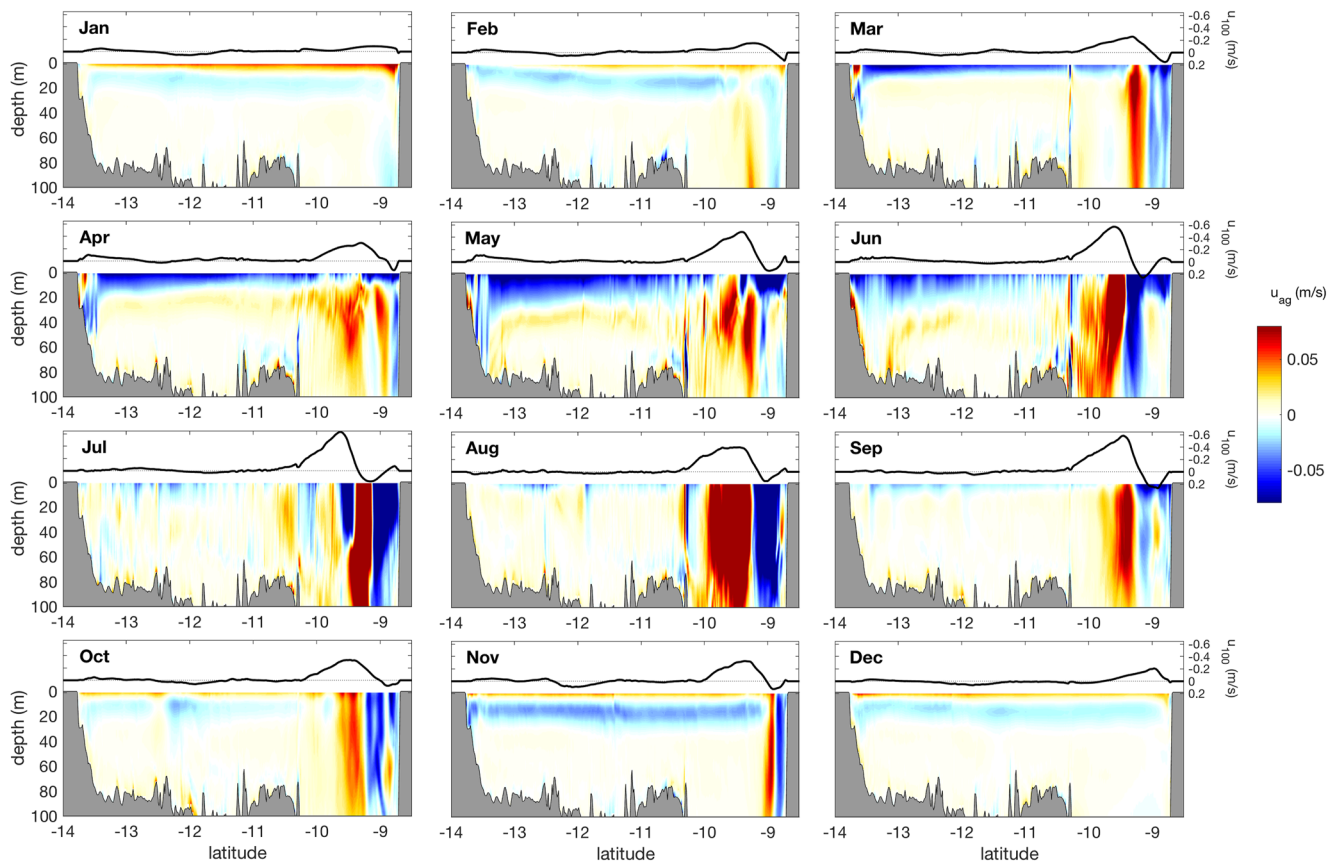


Figure 12. Monthly averages of the ageostrophic component of the zonal flow in m/s at 127°E in the top 100 m. Positive zonal flow (warm colors) is eastward and indicates a reduction of the Indonesian Throughflow. The black line at the top in each panel shows the full velocity field, also in m/s, at 100 m depth. Notice the vertical axis are reversed, with negative values at the top indicating westward flow. Near the northern boundary the ageostrophic velocity results from the curvature terms. Away from the northern boundary, within the top 20 m the ageostrophic velocities are capturing the Ekman flow.

The seasonal evolution of water masses measured by the moorings provides some evidence of this direct link between western route waters and the Timor throughflow (Figure 15). From February onwards the thermocline becomes shallower and the near surface waters become fresher. The freshening of the upper thermocline waters

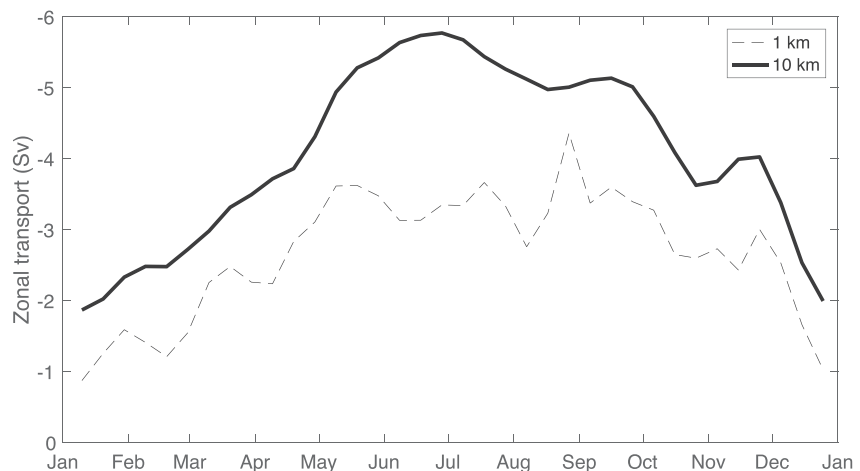


Figure 13. Zonal transport integrated in the top 150 m within the deep passage (north of 10°S) along 127°E. Negative values correspond to westward flow (positive transport in the Indonesian Throughflow sense). The vertical axis has been reversed. The thick black line shows results for the 10 km resolution model, and the dashed line for the 1 km resolution model.

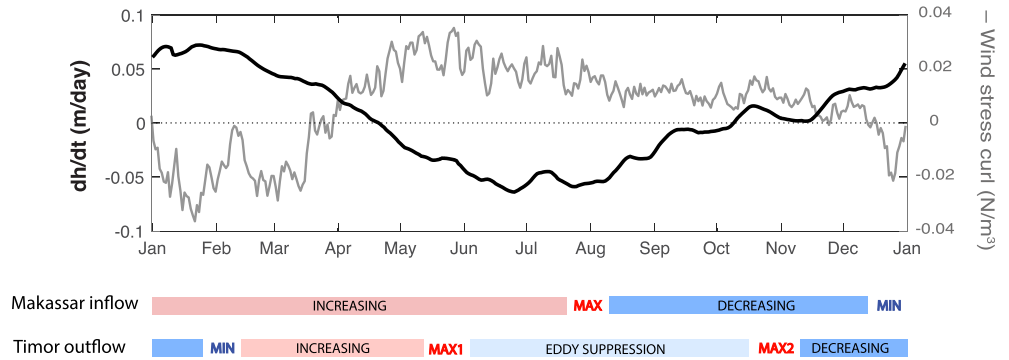


Figure 14. (Top) Time rate of change of Sea Surface Height (m/day, black) and wind stress curl (N/m^3 , gray) averaged in the Banda Sea (see box Figure 1). Note that the sign of the wind stress curl has been reversed so that positive (negative) indicates upwelling (downwelling). (Bottom) Schematic representation of the evolution of the thermocline transport in Makassar from Gordon et al. (2019) and Timor throughflow as per Figure 7.

is well documented both in Lombok (Sprintall et al., 2003) and Ombai (Molcard et al., 2001) straits. Atmadipoera et al. (2009) showed this fresh water signal originates in the Java Sea during the NWM monsoon, and progressively moves east reaching Lombok, Ombai and Timor 1, 3 and 5 months respectively after freshening peaks in the Java Sea. The increasing lag of this signal toward the east, and the fact that waters in the eastern Banda Sea remain saltier at all times than those observed in Timor, suggest that the fresh Java Sea water reaches Timor Passage without recirculating the Banda Sea. That is, it arrives via the western route (Figure 1).

Below 150 m, changes in T/S are more subtle. Nevertheless, salinity at middle depths becomes more vertically homogeneous during the SEM, when transport is large, consistent with a higher inflow of isohaline waters from the Banda Sea. During the NWM salinity minima and maxima develop at mid depth similar to those typically seen in the North Pacific influenced waters originating from Makassar Strait. We speculate that below 150 m waters may be subject to less recirculation and mixing during the NWM. The opposite timing between the export of Banda Sea water in the upper and intermediate layers would imply that convergence in one layer is balance by divergence in the other, consistent with the description of the circulation in Potemra et al. (2003) model analysis.

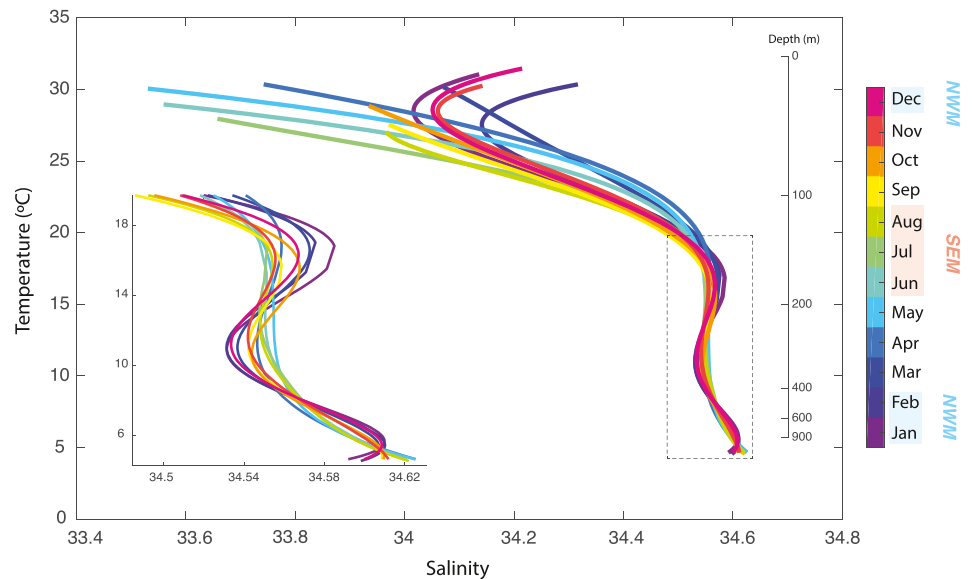


Figure 15. Monthly theta-S curves at the Sill mooring. Each curve is generated by fitting a 6th order polynomial to all data available in a given month. The vertical scale on the right side of the plot shows equivalent mean-depth values, obtained by binning time varying pressures in temperature intervals. It should be noted that the deepest salinity record available was located at 1000 m, so this diagram does not characterize the deepest flavors of Indonesian Throughflow water. On the left is a zoomed-in detail of the deeper part of the theta-S curve in the dashed box to the right.

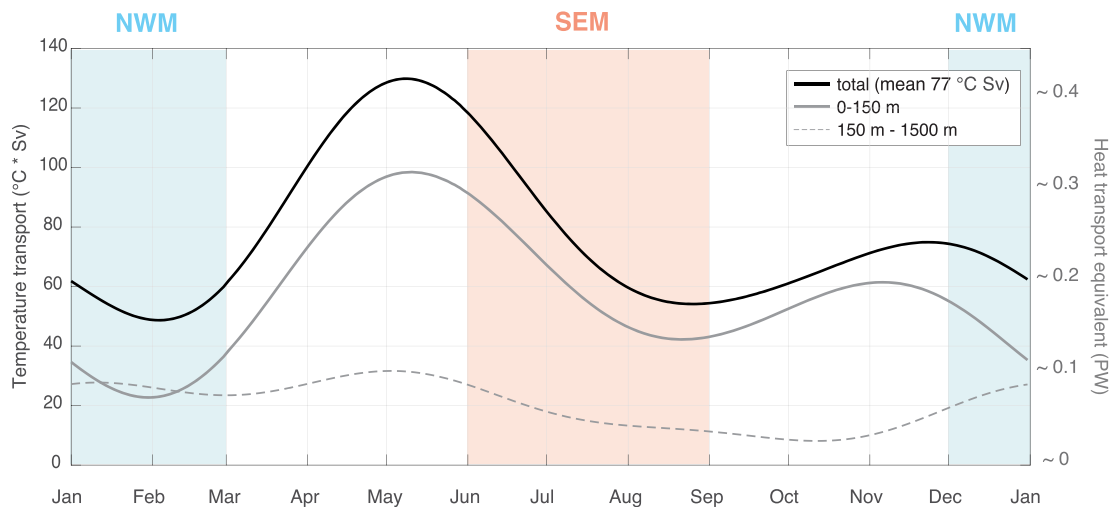


Figure 16. Seasonal cycle of the temperature transport in $^{\circ}\text{C Sv}$ by the Timor throughflow. Estimated from the gridded temperature and velocity fields derived by the moorings. On the right-side axis heat transport equivalent (PW) values are shown for an assumed return flow temperature of 3.4°C .

4.2. Non-linearities, “Gating” and Implications for Heat Transport

In summary, we contend that the overall seasonal cycle of transport in Timor Passage is modulated by the balance between the inflow of waters from Makassar and storage capacity in the internal seas. Between April and August, while the Banda Sea begins to discharge water and the inflow of Makassar progressively increases, we expect the transport in the upper layer in Timor to increase as well. However, non-linear local dynamics act to suppress the Timor throughflow in the upper layer after May when it is otherwise expected to be maximum. What is the fate of the water blocked by the eddies? One possibility is that, as proposed by Qu et al. (2008) in the context of Kelvin waves, the outflows control the cycles of convergence/divergence of the internal seas, and not the other way around. In which case changes in the rate of storage of the Banda Sea should follow changes in the transport at Timor. This relationship between Timor throughflow and SSH changes is not evident in our observations. Alternatively, the blocked waters at Timor contribute to enhanced transport in Ombai Passage. This is a much more likely scenario based on the satellite-derived surface geostrophic velocities. These show the transport originating in Ombai and entering the Indian Ocean through the Savu Sea is maximum between July and September (Figure 4), when both the altimeter and mooring records indicate a suppression of the flow at Timor.

It is possible that some of the variability associated with the eddies generated at the eastern part of the Timor Passage reaches the western part of the strait despite the constriction in the bathymetry. Variability in the 20–40 days band in the velocity records collected in Makassar Strait has been in fact attributed to eddies originating in the Sulawesi Sea that squeeze through the 40-km Labani Channel (Pujiana et al., 2012). The velocity records collected in Timor during the INSTANT experiment showed the flow in the northern and southern moorings was often anticorrelated, suggesting eddies may be present there despite the more laminar nature of the flow at their location (Sprintall et al., 2009). However, the magnitude of the seasonal cycle measured by INSTANT in Timor was smaller than reported here, consistent with the smaller amplitude of the seasonal cycle inferred at the nearby altimeter track. This reduction in the energy on seasonal time scales could be explained by the cycle of formation and dissipation of the eddies within the eastern section of the passage leading to energy cascading into higher frequencies.

Changes in the timing and pathway of the upper thermocline entering the Indian Ocean are likely to have a large impact on the heat carried by the ITF as temperature and velocity profiles in the ITF vary dramatically between locations and throughout the year. The surface intensified nature of the flow combined with the high SST values in the region result in a large portion of the heat being transported within the top layer of the ocean. For the Timor throughflow this means out of the 77°C Sv (equivalent to 0.25 PW for a 3.4°C reference temperature, see Tillinger & Gordon, 2010) transported by the top-to-bottom flow, 57°C Sv (0.2 PW heat transport equivalent) are transported within the top 150 m (Figure 16). The suppression of the upper thermocline flow by the eddies

that occurs during the June-August period results in a decrease in heat transport of more than half its peak value (approximately 0.2 PW) in just 3 months.

5. Conclusions

We have described the seasonal cycle of the Timor throughflow as observed by a 4.7-year long moored array deployed across the eastern end of Timor Passage combined with satellite observations and output from a high-resolution regional model of the Indonesian Seas. The flow structure across the strait and its seasonal cycle is surprisingly complex, due to a combination of the impacts of local winds driving seasonal upwelling, impinging remotely forced Kelvin waves and non-linear inertial effects on the source flow as it rounds the eastern tip of Timor Island, and forms anticyclonic eddies in the strait. As found in other ITF straits, the seasonal cycle also has distinct variations with depth.

The top-to-1500 m volume transport measured by the moored array follows a semi-annual pattern with maxima and minima occurring during both monsoon seasons. During the first half of the year, the flow above and below 300 m are more or less in phase, both leading to reduced transport in the late NWM (February) and enhanced flow in May, when the throughflow reaches peak strength (8 Sv). In the second half of the year variability in the deep flow, modulated by the arrival of Kelvin waves, dominates over the larger yet mostly steadier transport above. The overall minimum occurs during September and it is the result of the flow reversing at depth.

The transport in the upper thermocline (<150 m), which is relatively steady compared to the deep layer transport, is the largest and contributes the most to the total mean transport. The bulk of the upper thermocline transport occurs over the Timor Trench, the deep passage north of 10°S, with only a small contribution from the circulation over the shelf. The transport in this layer is smallest in February. A subsequent increase results from the balance between increasing inflow of North Pacific waters through Makassar strait driven by changes in the Indo-Pacific pressure gradient and a reduction of convergence followed by the onset of divergence in the Banda Sea driven by local winds. Both inflow from Makassar and divergence in the Banda Sea continue to increase throughout the SEM. However, the upper thermocline transport in Timor decreases from June onwards. Surface geostrophic velocities derived from altimetry across the eastern half of Timor Passage are in excellent agreement with the in situ observations. They show the decrease in transport is the result of an eastward flowing recirculation along the northern flank of the Timor Passage. Our model analysis shows this recirculation is the cumulative effect of eddies that develop in the eastern end of the strait due to strong non-linear local dynamics as the flow rounds the eastern tip of Timor.

Changes in amplitude and timing of the seasonal cycle of the surface geostrophic velocities on the western part of Timor Passage, as the throughflow approaches the Indian Ocean, confirm the idea that the suppression of the flow we observed at the mooring site is local in nature. However, implications of this local process are far reaching as they lead to a reduction of the temperature transported by the throughflow equivalent to 0.2 PW. Small scale processes such as those described here may be relevant to changes in the ITF on both shorter (e.g., intraseasonal) and longer (e.g., interannual to decadal) scales. Longer records of the volume and properties of the inflows and outflows of the ITF will be critical to understand the role played by small scales motions in the long-term evolution of the ITF and to improve our capacity to predict it.

Data Availability Statement

Mooring data was sourced from Australia's Integrated Marine Observing System (IMOS)—IMOS is enabled by the National Collaborative Research Infrastructure Strategy. The deep mooring data can be accessed through the AODN portal at <https://portal.aodn.org.au/search>. The data from the shallow moorings can be found at <https://data.aims.gov.au/moorings/IMOS-ITFIndonesianThroughflow/IMOS-ITFIndonesianThroughflow.html>. Altimetry data used in this study were developed, validated, and distributed by the CTOH/LEGOS, France. Version-2.0 vector wind analyses are produced by Remote Sensing Systems. Data are available at www.remss.com. Model output is archived at the Australian National Computing Facility.

Acknowledgments

B. Peña-Molino, B. M. Sloyan, M. Nikurashin, and O. Richet were supported by the Centre for Southern Hemisphere Oceans Research (CSHOR). CSHOR is a joint research Centre for Southern Hemisphere Ocean Research between QNLM and CSIRO. S. E. Wijffels was supported by the US National Science Foundation Grant No. OCE-1851333.

References

- Amante, C., & Eakins, B. W. (2008). *ETOPO1 1 Arc-minute global relief model: Procedures, data sources and analysis*. National Geophysical Data Center, NESDIS, National Oceanic and Atmospheric Administration, US Department of Commerce. 21.
- Atmadipoera, A., Molcard, R., Madec, G., Wijffels, S., Sprintall, J., Koch-Larrouy, A., et al. (2009). Characteristics and variability of the Indonesian Throughflow water at the outflow straits. *Deep Sea Research Part I: Oceanographic Research Papers*, 56(11), 1942–1954. <https://doi.org/10.1016/j.dsr.2009.06.004>
- Birol, F., Fuller, N., Lyard, F., Cancet, M., Nino, F., Delebecque, C., et al. (2017). Coastal applications from Nadir Altimetry: Example of the X-TRACK regional products. *Advances in Space Research*, 59(4), 936–953. <https://doi.org/10.1016/j.asr.2016.11.005>
- Clarke, A. J., & Liu, X. (1993). Observations and dynamics of semiannual and annual sea levels near the eastern equatorial Indian Ocean boundary. *Journal of Physical Oceanography*, 23(2), 3862–399. [https://doi.org/10.1175/1520-0485\(1993\)023<0386:oadosa>2.0.co;2](https://doi.org/10.1175/1520-0485(1993)023<0386:oadosa>2.0.co;2)
- Cresswell, G., Frische, A., Peterson, J., & Quadfasel, D. (1993). Circulation in the Timor Sea. *Journal of Geophysical Research*, 98(C8), 14379–14389. <https://doi.org/10.1029/93JC00317>
- Drushka, K., Sprintall, J., Gille, S. T., & Brodjonegoro, I. (2010). Vertical structure of Kelvin waves in the Indonesian Throughflow exit passages. *Journal of Physical Oceanography*, 40(9), 1965–1987. <https://doi.org/10.1175/2010JP04380.1>
- Feng, M., & Meyers, G. (2003). Interannual variability in the tropical Indian Ocean: A two-year time-scale of Indian Ocean Dipole. *Deep Sea Research Part II: Topical Studies in Oceanography*, 50(12–13), 2263–2284. [https://doi.org/10.1016/S0967-0645\(03\)00056-0](https://doi.org/10.1016/S0967-0645(03)00056-0)
- Feng, M., Zhang, N., Liu, Q., & Wijffels, S. (2018). The Indonesian Throughflow, its variability and centennial change. *Geoscience Letters*, 5(1), 1–10. <https://doi.org/10.1186/s40562-018-0102-2>
- Godfrey, J. S., & Mansbridge, J. V. (2000). Ekman transports, tidal mixing, and the control of temperature structure in Australia's northwest waters. *Journal of Geophysical Research*, 105(C10), 24021–24044. <https://doi.org/10.1029/2000JC900104>
- Gordon, A. L., & Fine, R. A. (1996). Pathways of water between the Pacific and Indian Oceans in the Indonesian seas. *Nature*, 379(6561), 146–149. <https://doi.org/10.1038/379146a0>
- Gordon, A. L., Napitu, A., Huber, B. A., Gruenburg, L. K., Pujiana, K., Agustadi, T., et al. (2019). Makassar Strait throughflow seasonal and interannual variability: An overview. *Journal of Geophysical Research: Oceans*, 124(6), 3724–3736. <https://doi.org/10.1029/2018JC014502>
- Gordon, A. L., & Susanto, R. D. (2001). Banda Sea surface-layer divergence. *Ocean Dynamics*, 52(1), 2–10. <https://doi.org/10.1007/s10236-001-8172-6>
- Hu, D., Wu, L., Cai, W., Gupta, A. S., Ganachaud, A., Qiu, B., et al. (2015). Pacific Western boundary currents and their roles in climate. *Nature*, 522(7556), 299–308. <https://doi.org/10.1038/nature14504>
- Hu, S., & Sprintall, J. (2017). Observed strengthening of interbasin exchange via the Indonesian seas due to rainfall intensification. *Geophysical Research Letters*, 44(3), 1448–1456. <https://doi.org/10.1002/2016GL072494>
- Kiss, A. E., Hogg, A. M., Hannah, N., Boeira Dias, F., Brassington, G. B., Chamberlain, M. A., et al. (2020). ACCESS-OM2 v1. 0: A global ocean–Sea Ice model at three resolutions. *Geoscientific Model Development*, 13(2), 401–442. <https://doi.org/10.5194/gmd-13-401-2020>
- Lee, S. K., Park, W., Baringer, M. O., Gordon, A. L., Huber, B., & Liu, Y. (2015). Pacific origin of the abrupt increase in Indian Ocean heat content during the warming hiatus. *Nature Geoscience*, 8(6), 445–449. <https://doi.org/10.1038/ngeo2438>
- Lee, T., Awaji, T., Balmaseda, M., Ferry, N., Fujii, Y., Fukumori, I., et al. (2010). Consistency and fidelity of Indonesian-throughflow total volume transport estimated by 14 ocean data assimilation products. *Dynamics of Atmospheres and Oceans*, 50(2), 201–223. <https://doi.org/10.1016/j.dynatmoce.2009.12.004>
- Marshall, J., Adcroft, A., Hill, C., Perelman, L., & Heisey, C. (1997). A finite-volume, incompressible Navier Stokes model for studies of the ocean on parallel computers. *Journal of Geophysical Research*, 102(C3), 5753–5766. <https://doi.org/10.1029/96JC02775>
- Molcard, R. M., Fieux, M., & Syamsudin, F. (2001). The throughflow within Ombai Strait. *Deep-Sea Research*, 48(5), 1237–1253. [https://doi.org/10.1016/S0967-0637\(00\)00084-4](https://doi.org/10.1016/S0967-0637(00)00084-4)
- Murtugudde, R., Busalacchi, A. J., & Beauchamp, J. (1998). Seasonal-to-interannual effects of the Indonesian Throughflow on the tropical Indo-Pacific Basin. *Journal of Geophysical Research*, 103(C10), 21425–21441. <https://doi.org/10.1029/98JC02063>
- Potemra, J. T. (1999). Seasonal variations of upper ocean transport from the Pacific to the Indian Ocean via Indonesian straits. *Journal of Physical Oceanography*, 29(11), 2930–2944. [https://doi.org/10.1175/1520-0485\(1999\)029<2930:vouout>2.0.co;2](https://doi.org/10.1175/1520-0485(1999)029<2930:vouout>2.0.co;2)
- Potemra, J. T., Hautala, S. L., & Sprintall, J. (2003). Vertical structure of Indonesian Throughflow in a large-scale model. *Deep Sea Research Part II: Topical Studies in Oceanography*, 50(12–13), 2143–2161. [https://doi.org/10.1016/S0967-0645\(03\)00050-X](https://doi.org/10.1016/S0967-0645(03)00050-X)
- Potemra, J. T., Hautala, S. L., Sprintall, J., & Pandoe, W. (2002). Interaction between the Indonesian Seas and the Indian Ocean in observations and numerical models. *Journal of Physical Oceanography*, 32(6), 1838–1854. [https://doi.org/10.1175/1520-0485\(2002\)032<1838:ibtisa>2.0.co;2](https://doi.org/10.1175/1520-0485(2002)032<1838:ibtisa>2.0.co;2)
- Pujiana, K., Gordon, A. L., Metzger, E. J., & Field, A. L. (2012). The Makassar Strait pycnocline variability at 20–40 days. *Dynamics of Atmospheres and Oceans*, 53, 17–35. <https://doi.org/10.1016/j.dynatmoce.2012.01.001>
- Pujiana, K., McPhaden, M. J., Gordon, A. L., & Napitu, A. M. (2019). Unprecedented response of Indonesian Throughflow to anomalous Indo-Pacific climatic forcing in 2016. *Journal of Geophysical Research: Oceans*, 124(6), 3737–3754. <https://doi.org/10.1029/2018jc014574>
- Qu, T., Du, Y., McCreary, J. P., Jr., Meyers, G., & Yamagata, T. (2008). Buffering effect and its related ocean dynamics in the Indonesian Throughflow region. *Journal of physical oceanography*, 38(2), 503–516. <https://doi.org/10.1175/2007JPO3759.1>
- Qu, T., Meyers, G., Godfrey, J. S., & Hu, D. (1994). Ocean dynamics in the region between Australia and Indonesia and its influence on the variation of sea surface temperature in a global general circulation model. *Journal of Geophysical Research*, 99(C9), 18433–18445. <https://doi.org/10.1029/94JC00858>
- Ridgway, K. R., & Godfrey, J. S. (2015). The source of the Leeuwin Current seasonality. *Journal of Geophysical Research: Oceans*, 120(10), 6843–6864. <https://doi.org/10.1002/2015JC011049>
- Schiller, A., Wijffels, S. E., Sprintall, J., Molcard, R., & Oke, P. R. (2010). Pathways of intraseasonal variability in the Indonesian Throughflow region. *Dynamics of Atmospheres and Oceans*, 50(2), 174–200. <https://doi.org/10.1016/j.dynatmoce.2010.02.003>
- Sen Gupta, A., McGregor, S., Van Sebille, E., Ganachaud, A., Brown, J. N., & Santoso, A. (2016). Future changes to the Indonesian Throughflow and Pacific circulation: The differing role of wind and deep circulation changes. *Geophysical Research Letters*, 43(4), 1669–1678. <https://doi.org/10.1002/2016GL067757>
- Sprintall, J., Gordon, A. L., Murtugudde, R., & Susanto, R. D. (2000). A semiannual Indian Ocean forced Kelvin wave observed in the Indonesian seas in May 1997. *Journal of Geophysical Research*, 105(C7), 17217–17230. <https://doi.org/10.1029/2000JC900065>
- Sprintall, J., Gordon, A. L., Wijffels, S. E., Feng, M., Hu, S., Koch-Larrouy, A., et al. (2019). Detecting change in the Indonesian seas. *Frontiers in Marine Science*, 6, 257. <https://doi.org/10.3389/fmars.2019.00257>
- Sprintall, J., & Liu, W. T. (2005). Ekman mass and heat transport. *Oceanography*, 18(4), 88. <https://doi.org/10.5670/oceanog.2005.09>

- Sprintall, J., Potemra, J. T., Hautala, S. L., Bray, N. A., & Pandoe, W. W. (2003). Temperature and salinity variability in the exit passages of the Indonesian Throughflow. *Deep Sea Research Part II: Topical Studies in Oceanography*, 50(12–13), 2183–2204. [https://doi.org/10.1016/S0967-0645\(03\)00052-3](https://doi.org/10.1016/S0967-0645(03)00052-3)
- Sprintall, J., & Révelard, A. (2014). The Indonesian Throughflow response to Indo-Pacific climate variability. *Journal of Geophysical Research: Oceans*, 119(2), 1161–1175. <https://doi.org/10.1002/2013JC009533>
- Sprintall, J., Wijffels, S. E., Molcard, R., & Jaya, I. (2009). Direct estimates of the Indonesian Throughflow entering the Indian ocean: 2004–2006. *Journal of Geophysical Research*, 114(C7), C07001. <https://doi.org/10.1029/2008JC005257>
- Susanto, R. D., Moore, T. S., & Marra, J. (2006). Ocean color variability in the Indonesian Seas during the SeaWiFS era. *Geochemistry, Geophysics, Geosystems*, 7(5), Q05021. <https://doi.org/10.1029/2005GC001009>
- Susanto, R. D., & Song, Y. T. (2015). Indonesian Throughflow proxy from satellite altimeters and gravimeters. *Journal of Geophysical Research: Oceans*, 120(4), 2844–2855. <https://doi.org/10.1002/2014JC010382>
- Tillinger, D., & Gordon, A. L. (2010). Transport weighted temperature and internal energy transport of the Indonesian Throughflow. *Dynamics of Atmospheres and Oceans*, 50(2), 224–232. <https://doi.org/10.1016/j.dynatmoce.2010.01.002>
- Wentz, F. J., Scott, J., Hoffman, R., Leidner, M., Atlas, R., & Ardizzone, J. (2015). *Remote Sensing Systems Cross-Calibrated Multi-Platform (CCMP) 6-hourly ocean vector wind analysis product on 0.25 deg grid Version 2.0*. Remote Sensing Systems. Retrieved from www.remss.com/measurements/ccmp
- Wijffels, S. E., Beggs, H., Griffin, C., Middleton, J. F., Cahill, M., King, E., et al. (2018). A fine spatial-scale sea surface temperature atlas of the Australian regional seas (SSTAARS): Seasonal variability and trends around Australasia and New Zealand revisited. *Journal of Marine Systems*, 187, 156–196. <https://doi.org/10.1016/j.jmarsys.2018.07.005>
- Wyrtki, K. (1987). Indonesian through flow and the associated pressure gradient. *Journal of Geophysical Research*, 92(C12), 12941–12946. <https://doi.org/10.1029/JC092iC12p12941>
- Zhang, Y., Feng, M., Du, Y., Phillips, H. E., Bindoff, N. L., & McPhaden, M. J. (2018). Strengthened Indonesian Throughflow drives decadal warming in the southern Indian Ocean. *Geophysical Research Letters*, 45(12), 6167–6175. <https://doi.org/10.1029/2018GL078265>